ACADEMIC PRESS

Available online at www.sciencedirect.com
SCIENCE DIRECT®

Icarus 164 (2003) 317–333

ICARUS

www.elsevier.com/locate/icarus

Tremolite decomposition on Venus II. Products, kinetics, and mechanism

Natasha M. Johnson [a,b,*] and Bruce Fegley Jr. [a]

[a] *Planetary Chemistry Laboratory, Department of Earth and Planetary Sciences, Washington University, Campus Box 1169, St. Louis, MO 63130, USA*
[b] *NASA Goddard Space Flight Center, Laboratory for Extraterrestrial Physics, Code 691, Greenbelt, MD 20771, USA*

Received 8 March 2002; revised 24 February 2003

Abstract

We present revised tremolite powder thermal decomposition kinetics using previous and newly acquired data from longer time (years instead of months) and lower temperature experiments (< 1073 K). We also present kinetic results for decomposition of millimeter- to centimeter-sized tremolite grains. Natural tremolite samples were heated at ambient pressure in flowing CO_2 or N_2 gas from 1023–1238 K. The tremolite decomposition products are a physical mixture of two pyroxene solid solutions (with the bulk composition $Dp_{59}En_{41}$), a silica polymorph, and water vapor. Decomposition rates were calculated by using the mass loss of the heated samples. Tremolite crystals and crystalline powder decompositions follow different but related Avrami–Erofe'ev (nucleation and growth) kinetic models. The rate equations for thermal decomposition of tremolite crystalline powder and the larger crystal grains are $\log_{10} k_{\text{powder}}\ (\text{h}^{-1}) = 18.69(\pm 0.19) - 23{,}845(\pm 833)/T$ and $\log_{10} k_{\text{crystal}}\ (\text{h}^{-1}) = 19.82(\pm 0.07) - 25{,}670(\pm 916)/T$. The associated apparent activation energies are $456(\pm 16)$ kJ mol^{-1} and $491(\pm 18)$ kJ mol^{-1}, respectively. We propose a decomposition mechanism and suggest that decomposition and dehydroxylation occur simultaneously. The rate-limiting step is proposed to be structural rearrangement of the amphibole structure to the two pyroxenes and silica. This step and the overall decomposition rate are predicted to be independent of pressure from 1 to 100 bars. These kinetic analyses strengthen our previous conclusion (Johnson and Fegley, 2000, Icarus 146, 301–306) that if hydrous minerals, such as tremolite, formed on Venus during a wetter past, then these minerals could still exist at current conditions on Venus' surface today.

Keywords: Venus; Mineralogy; Tremolite; Kinetics; Mechanism

Introduction

Hydrous minerals, such as amphiboles, play important roles in terrestrial geology from being characteristic late formation minerals in contact and regionally metamorphosed rocks to incorporating or releasing water in subduction zones. There are numerous studies about amphiboles yet surprisingly few that address amphibole thermal decomposition rates. Amphibole thermal decomposition kinetics studies have been generally limited to asbestos minerals that have commercial value such as crocidolite (fibrous riebeckite) or amosite (fibrous grunerite) (e.g., Hodgson, 1965; Hodgson et al., 1965; Freeman, 1966; Clark, 1966; Clark and Freeman, 1967; Ghose, 1981). However, thermal decomposition of amphiboles is also important for understanding the mineralogy of Venus' surface.

As discussed by us previously (Johnson and Fegley, 2000a), if there had been more water in Venus' past, then hydrous minerals such as amphiboles and micas may have formed on or within the surface. The high deuterium/hydrogen ratio in Venus' atmosphere suggests that Venus may have once had a greater abundance of water (Donahue et al., 1997). If so, the detection of hydrous minerals on Venus would prove that Venus had more water in the past. Equilibrium thermodynamic calculations predict that amphiboles and micas decompose under current Venus surface conditions (Zolotov et al., 1997). Thermodynamic calculations provide information on mineral stabilities under specific environmental conditions. However, these calculations do not provide any information on the rate at which a mineral assemblage will transform or decompose under those conditions. Such data can only be obtained experimentally.

We previously studied thermal decomposition of tremolite, an amphibole with the ideal formula of $Ca_2Mg_5Si_8O_{22}(OH)_2$, at 1073–1238 K and concluded that it does not de-

* Corresponding author.
E-mail address: njohnson@lepvax.gsfc.nasa.gov (N.M. Johnson).

0019-1035/$ – see front matter
doi:10.1016/S0019-1035(03)00102-7

compose at Venus' surface temperatures (Johnson and Fegley, 2000a, 2000b). We continued these and additional experiments at lower temperatures (50 degrees cooler), longer times (years versus months), and for larger grain sizes (millimeter- to centimeter-sized grains versus powder). Further analysis of the data also showed that a different (though related) kinetic model was more appropriate for the powder decomposition data.

In this paper, we

(1) review our experimental method,
(2) identify and describe the decomposition products,
(3) give an analysis of the kinetic data and present a new decomposition rate and activation energy,
(4) propose a mechanism using characterizations of the reacted samples, kinetic data, and literature activation energy data for cation and oxygen diffusion, and lastly,
(5) discuss implications of these results for Venus.

1. Experiments

The experiments reported here follow the same methods as described in Johnson and Fegley (2000a). We used tremolite that originated from Canaan, Connecticut (purchased from Ward's Natural Science Company). Table 1 lists the chemical composition of ideal tremolite, Canaan tremolite, decomposed Canaan tremolite, and decomposed ideal tremolite. The chemical formula of the Canaan tremolite calculated from our electron microprobe analyses is $K_{0.01}(Ca_{1.94}Na_{0.04})(Mg_{4.90}Fe_{0.02})(Si_{7.98}Al_{0.03})O_{22}(OH)_{2.20}$, based on 24(O,OH,F). The water content was calculated by measuring the mass loss of three samples that were completely devolatilized at 1273 K. All the mass loss was due to water loss (Johnson and Fegley, 2000a).

Table 1
Tremolite chemical analyses

Oxides	Ideal	Tremolite[a] from Canaan, CT		Decomposed
	tremolite	Initial 10 pts ($\pm1\sigma$)	Decomposed[b] 11 pts ($\pm1\sigma$)	ideal tremolite
SiO_2	59.20	58.72 (0.30)	59.10 (0.80)	60.51
TiO_2		b.d.l.	b.d.l.	
Al_2O_3		0.22 (0.06)	0.20 (0.04)	
Cr_2O_3		b.d.l.	b.d.l.	
FeO		0.21 (0.03)	0.21 (0.05)	
MnO		b.d.l	b.d.l.	
MgO	24.80	24.20 (0.15)	25.02 (0.37)	25.37
CaO	13.80	13.29 (0.11)	13.47 (0.42)	14.12
Na_2O		0.15 (0.05)	0.15 (0.03)	
K_2O		0.08 (0.04)	0.04 (0.02)	
H_2O	2.20	2.426 (0.041)[c]	–	
F		b.d.l.	b.d.l.	
Total	100.00	99.30	98.19	100.00

b.d.l.: analyzed—considered below detection limits ($1\sigma \geqslant$ measured value < 0.10 wt%).

[a] Microprobe analyses of tremolite powder used in this study.

[b] Completely decomposed tremolite[a] (46 h, 1000° C).

[c] Determined by heating three tremolite[a] samples at $\sim$ 1000° C and measuring mass loss (1σ).

We isolated tremolite grains that had no visible impurities and ground a portion of these grains into powder. We heated two types of tremolite samples: powder and larger crystalline grains. Powder samples consisted of many micrometer-sized crystallites and the larger crystalline grain samples contained several millimeter- to centimeter-sized grains as multicrystalline chunks. The average initial mass of each sample was approximately 100 mg. We heated each sample under continuous gas flow using either instrument grade CO_2 (99.99%) or ultra-high-purity (UHP) N_2 (99.999%). The linear flow rates used were ~ 3 cm min^{-1} at standard temperature (25° C) and pressure (1 bar). Before and after heating, the tremolite sample and its container (an alumina combustion boat or an alumina crucible) were weighed on an analytical balance (with an accuracy of ±1 μg). Each sample was heated and weighed until mass loss reached a plateau. Samples were heated at constant temperatures ranging from 1023 to 1238 K for times of 1 hour to over 3 years. The experimental data are given in Appendix A (Tables A.1–A.5).

We analyzed samples by X-ray diffraction (XRD), electron microscopy (EMP), scanning electron microscopy (SEM), infrared spectroscopy, and optical microscopy. Additional details of the sample preparation and analytical procedures are given in Johnson and Fegley (2000a).

2. Tremolite decomposition products

When heated, tremolite decomposes into two pyroxenes (enstatite and diopside), silica, and water vapor as follows (Deer et al., 1997):

$$\underset{\text{tremolite}}{Ca_2Mg_5Si_8O_{22}(OH)_2} = \underset{\text{diopside}}{2CaMgSi_2O_6} + \underset{\text{enstatite}}{3MgSiO_3} + \underset{\text{silica}}{SiO_2} + H_2O\ (\text{gas}). \quad (1)$$

Using infrared spectroscopy, we confirmed the loss of water from the tremolite structure during decomposition (Johnson and Fegley, 2000a). Pyroxenes form during tremolite decomposition but not as pure endmembers as suggested by Eq. (1). Posnjak and Bowen (1931) first established that the resulting pyroxenes did not have pure endmember compositions. The bulk chemical composition of the pyroxene product represented in Eq. (1) can be expressed in several equivalent ways: $5MgSiO_3{\cdot}2CaSiO_3$, $Ca_2Mg_5Si_7O_{21}$, as a combination of 60 mol% enstatite and 40 mol% diopside, or as a combination of 41 wt% enstatite plus 59 wt% diopside ($Dp_{59}En_{41}$). In this paper, we use $Dp_{59}En_{41}$ to represent the pyroxene product bulk composition.

Figure 1 shows the enstatite–diopside phase diagram with the composition $Dp_{59}En_{41}$ plotted within the two-phase field of this diagram. The compositions of the two pyroxenes in the physical mixture fall along the sides of the solvus and depend on temperature. The proportions of the two pyroxenes in the physical mixture are calculated using the lever

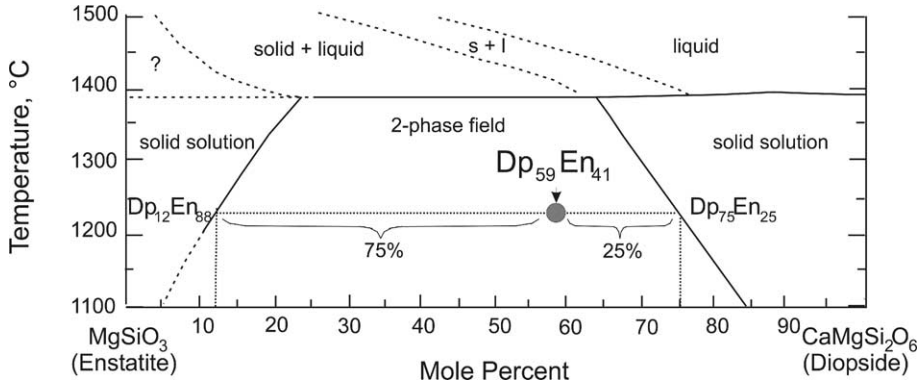

Fig. 1. An example of an enstatite ($MgSiO_3$)–diopside ($CaMgSi_2O_6$) phase diagram at one atmosphere of pressure. The position of $Dp_{59}En_{41}$ is indicated with a solid circle and the proportions and compositions of the solid-solution pyroxene phases are labeled. This diagram is a scaled down version modified from Boyd and Schairer (1964). A pyroxene phase diagram at lower temperatures is given by Carlson (1986).

rule. For example, at 1235° C (1508 K) the $Dp_{59}En_{41}$ bulk composition corresponds to the mixture of 25 wt% Mg-rich pyroxene ($Dp_{12}En_{88}$) and 75 wt% Ca-rich pyroxene ($Dp_{75}En_{25}$).

Decomposed tremolite is porous and fine-grained (e.g., see Johnson and Fegley, 2000a, Fig. 4b) and electron microprobe analyses give a bulk composition that agrees with the values calculated using Eq. (1) (see Table 1). However, electron microprobe methods cannot distinguish between the compositions of the individual phases because the product is so fine-grained. X-ray diffraction is needed to identify the pyroxenes and the silica phase.

Pyroxene identification. We attempted to identify the pyroxene products via XRD by comparing the decomposed tremolite against a physical mixture of pure enstatite and diopside. However, this comparison did not give a satisfactory match. We then synthesized pyroxene with the bulk composition of $Dp_{59}En_{41}$ by mixing and heating stoichiometric proportions of reagent grade $CaCO_3$, $Mg(OH)_2$, and silica. We followed a heating procedure similar to that used by Boyd and Schairer (1964). The reactants were heated to 1400° C (1673 K) for 1.25 h to achieve partial melting, cooled to ∼ 1235° C (1508 K), and held at this lower temperature for 50 days. We used this temperature of 1235° C to ensure that the reagents completely reacted and would equilibrate in a reasonable length of time.

Electron microprobe analysis and XRD showed that we produced a pyroxene product with the correct bulk composition. Figure 2 shows XRD patterns of the tremolite sample, tremolite heated at 1235° C (1508 K), and the $Dp_{59}En_{41}$ pyroxene produced at ∼ 1235° C (1508 K).

The XRD *d*-spacings of the decomposed tremolite and $Dp_{59}En_{41}$ pyroxene are in good agreement. This result agrees with the earlier work of Posnjak and Bowen (1931) who also compared synthesized pyroxene to decomposed tremolite. We used this $Dp_{59}En_{41}$ XRD pattern to confirm formation of pyroxene in tremolite that had decomposed at cooler temperatures. Although the synthesized pyroxene was made at a temperature 250 degrees higher than the hottest

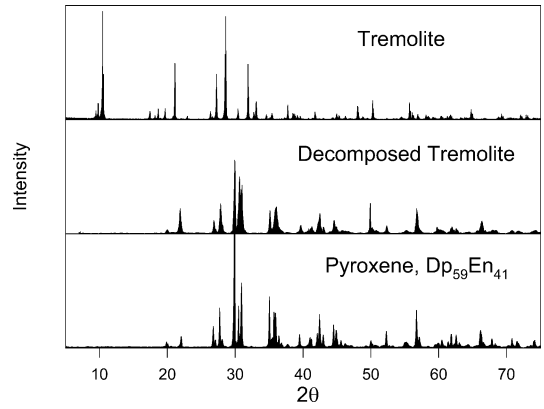

Fig. 2. X-ray diffraction patterns of tremolite, tremolite decomposed at 1235° C (1508 K), and pyroxene, $Dp_{59}En_{41}$, synthesized at ∼ 1235° C (∼ 1508 K).

tremolite kinetic experiment, its XRD pattern proved to be a more accurate reference than that produced by the physical mixture of pyroxene endmembers mentioned earlier. The pyroxene XRD data needed to determine the proportions and compositions of pyroxenes in the decomposed tremolite are not currently available.

Silica identification. Three silica polymorphs are stable at atmospheric pressure: quartz (up to 1140 K), tridymite (1140 to 1743 K), and cristobalite (1743 K to the melting point of 1996 K) (Sosman, 1965). Each is metastable within the other temperature ranges. Based on these temperatures, we expect that tridymite would be the resulting silica phase in about half of our decomposition experiments. However, identification of the silica phase by XRD in the decomposition products was inconclusive (Johnson, 2002). Either the main peak positions of these silica phases were overlapped by pyroxene and/or the peak intensities were too low to be distinguished from the background noise. Silica forms 10% by volume of the decomposition products shown in Eq. (1). This small volume lowers the overall intensity of the resulting silica XRD pattern and could prevent detection of lower intensity peaks.

Table 2
Summary of literature studies of tremolite thermal decomposition

Reference	Temperature (° C)	Purpose, method(s), and results
Posnjak and Bowen (1931)	115–1100	Water content, loss of adsorbed and structural water as a function of temperature, heated in air, structural water loss occurs between 750 and 1000° C, XRD, optical microscopy, no rate data *Product*(*s*): solid solution pyroxene from diopside–clinoenstatite series ($2CaSiO_3{\cdot}5MgSiO_3$) and cristobalite
Thilo (1939)	1100	XRD study, heated in air(?) for 72 h, no rate data *Product*(*s*): $MgSiO_3$-diopside solid solution and cristobalite (apparently disordered)
Wittels (1951)	100–1050	Differential thermal analyses (DTA) study, XRD, optical microscopy, tremolite *c*-axis contracts at 825° C, irreversible transformation, evolves 2.76 cal g^{-1} (11.55 J g^{-1}), no rate data *Product*(*s*): not specified
Wittels (1952)	600–1125	DTA study, XRD, optical microscopy, $\Delta H = 6.4$ cal g^{-1} (26.8 J g^{-1}) $\pm$ 15%, structural disintegration occurred between 925 and 1125° C, no rate data *Product*(*s*): pseudomorph of pyroxene and cristobalite after amphibole
Vermaas (1952)	0–1200	DTA study, XRD, optical microscopy, electron microscopy, structural water loss at 930–988° C, exothermic peaks between 815 and 824° C, no rate data *Product*(*s*): pseudomorph of clinopyroxene ($2CaSiO_3{\cdot}5MgSiO_3$) and cristobalite after tremolite
Freeman and Taylor (1960)	200–1100	Determine weight-loss curve, heated in N_2, XRD, optical microscopy, proposed detailed mechanism, no rate data *Product*(*s*): pyroxene, one phase (possibly similar to clinopyroxene), no cristobalite
Freeman (1962)	200–1100	Chapter from PhD thesis, same as Freeman and Taylor (1960)
Freeman (1966)	100–1200	Compare weight-loss curve of tremolite dehydroxylation to those of other hydrous Mg-bearing minerals *Product*(*s*): not specified
Patterson and O'Conner (1966)	600–1000	Infrared absorption study, XRD, heated in air for 1 h, no rate data *Product*(*s*): pyroxene at 1000° C, no change at lower temperatures
Xu et al. (1996)	700–780	Transmission electron microscopy (TEM) study, proposed mechanism but no rate data *Product*(*s*): two clinopyroxenes, one of which is silica enriched (chemical formulas based on EMP analyses), surficial amorphous silica
Johnson and Fegley (2000a, 2000b)	800–965	Isothermal weight-loss study, crystalline powder heated in CO_2 or N_2, SEM, XRD, electron microprobe, infrared spectroscopy, rate data, rate equation, apply results to Venus surface temperatures *Product*(*s*): not specified
Johnson and Fegley (2003)	905–981	Isothermal weight-loss study, gravimetric data for fluorine-bearing tremolite powder heated in CO_2, XRD, SEM, electron microscopy, rate equation, apply results to Venus surface temperatures *Product*(*s*): mixture of two solid-solution pyroxenes, high-temperature silica phase
This work	750–965	Isothermal weight-loss study, gravimetric data for crystalline powder and crystals heated in CO_2 or N_2, XRD, SEM, electron microscopy, rate data, discussion of decomposition products, kinetics and mechanism *Product*(*s*): mixture of two solid-solution pyroxenes, silica polymorph (see text)

Identification of the silica phase in the tremolite decomposition products is also unclear in the previous tremolite thermal decomposition studies listed in Table 2. Only Posnjak and Bowen (1931) and Thilo (1939) identified and characterized a distinct silica phase, cristobalite, in the tremolite decomposition products. The remaining studies either did not detect silica or did not give details about their identification process. Xu et al. (1996) reported the formation of surficial amorphous SiO_2 on their decomposed tremolite sample and a silica-rich pyroxene. Freeman and Taylor (1960) and Freeman (1962) attributed the absence of a silica product to a short heating period (5 h) that did not allow enough time for silica formation. Another possibility is that a silica phase formed but was too small to be detected. This may have also been the case with Patterson and O'Conner (1966) and Xu et al. (1996) who may not have heated their tremolite samples long enough (1 and 10 h, respectively) to form a silica phase or formed enough crystalline silica to be detected. Pyroxene cannot host all the resulting SiO_2 because stoichiometric single-chain silicates cannot accommodate more than two silicon atoms per formula unit (Klein and Hurlbut, 1993). It is reasonable to expect that a silica polymorph forms during tremolite decomposition if given enough time at high temperature.

3. Kinetic results

As in Johnson and Fegley (2000a, 2000b, 2003), we determined the tremolite decomposition kinetics by using mass loss to measure the extent of reaction as a function of time. The fraction reacted of tremolite, α, varies from 0 to 1 and is calculated as

$$\alpha = \left(\frac{\Delta m}{m_i} \cdot \frac{1}{\delta_{\max}} \right), \tag{2}$$

where Δm is the mass change, m_i is the initial mass, and $\delta_{\max}$ is the maximum possible fractional mass loss. Here $\delta_{\max}$ is 0.02426 as determined by complete decomposition at

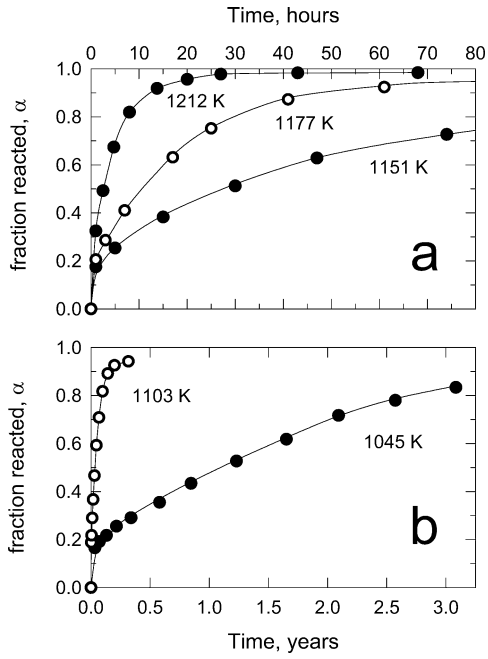

Fig. 3. Typical weight loss curves for tremolite powder decomposition. The fraction reacted, α, is calculated from the mass loss (see text for details) and is plotted here as a function of time. These samples were heated under the same experimental conditions (CO_2 gas, horizontal furnaces, cylindrical crucibles).

1273 K (Johnson and Fegley, 2000a). The fractions reacted (α) for all experiments are listed in Appendix A, Tables A.1–A.5. Representative plots in Fig. 3 show the fraction reacted as a function of time and illustrate that samples heated at lower temperatures take longer to decompose.

To determine if tremolite decomposition follows the same kinetic behavior at all temperatures studied, we plot the fraction reacted, α, of all the experiments as a function of reduced time. Reduced time is time normalized to 50% decomposition time ($t_{\text{reduced}} = t/t_{0.5}$). If the kinetic behavior is the same for all conditions then the reduced data should plot along the same curve. Figure 4 shows reduced time plots for two different cases:
(a) powder experiments only, and
(b) powder and tremolite crystal experiments.
Figure 4a shows that the kinetic behavior is the same for tremolite powder under different experimental conditions.

However, similar kinetic behavior is not observed between powder and crystals as shown by the reduced time data in Fig. 4b. There are two major differences between the powder and crystal data. First, there is a slope difference between the curves for the different data sets; second, the crystal kinetic data deviate more from the overall data trend as the fraction reacted approaches unity. This deviation indicates a change in mechanism or kinetic process. This difference in kinetic behavior between tremolite powder and tremolite crystals is not unexpected because of the different size of the samples, i.e., micrometer- versus millimeter-sized grains, and is addressed when we discuss the kinetic models for the rate equation calculations.

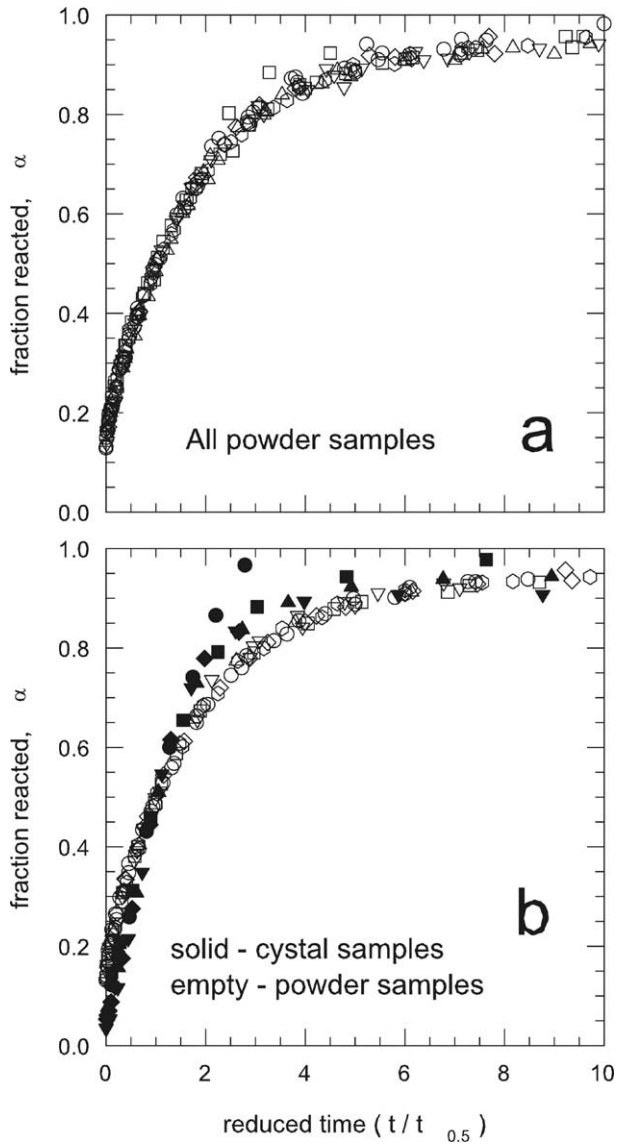

Fig. 4. Reduced time plots that show the fraction reacted, α, of the samples with reduced time. Reduced time is time normalized to 50% decomposition time ($t_{\text{reduced}} = t/t_{0.5}$).

We determined the reaction kinetics by fitting data to kinetic models via linear regressions. As discussed by Brown et al. (1980) the selected model should give an accurate description of the reaction process and make an acceptable linear regression to the majority of the data. We evaluated a number of models but only four meet these criteria. These four models are nucleation and growth, contracting volume, diffusion, and first-order reaction. The nucleation and growth models, also known as Avrami–Erofe'ev models, are represented by the equation

$$f(\alpha) = \left(-\ln(1-\alpha)\right)^{1/n}, \tag{3}$$

where $n = \beta + \lambda$. β describes nucleation as a function of time (i.e., exponential ($0 < \beta < 1$), linear ($\beta = 1$), and instantaneous ($\beta = 0$)) and λ gives the dimensional growth of the nuclei ($\lambda = 1, 2, 3$). The contracting volume model,

with $f(\alpha) = 1 - (1-\alpha)^{1/3}$, accounts for decreasing unreacted volume with time. The diffusion model is similar to the contracting volume model except that it includes movement of a species through a reacted interface. The Ginstling–Brounshtein model represented by $f(\alpha) = 1 - (2\alpha/3) - (1-\alpha)^{2/3}$, accounts for diffusion through a reacted interface of decreasing size. The first-order reaction model, $f(\alpha) = -\ln(1-\alpha)$, commonly associated with gas-phase reactions and radioactive decay, is a form of the Avrami–Erofe'ev model, Eq. (3), where $n = 1$. Decomposition of fine powders can generally be described by using the first-order model (Galwey and Brown, 1999). Descriptions of these and other models can be found in any good text about decomposition kinetics of solids (e.g., Brown et al., 1980; Galwey and Brown, 1999).

In an ideal system, one model could describe a reaction from beginning to end but in real life a reaction may follow a different kinetic model at each reaction stage. In many kinetic analyses a selected range of values is used to determine the overall reaction rate (Galwey and Brown, 1999). We calculated linear regressions of $f(\alpha)$ versus time for each model for several different data ranges but did not include data where $\alpha > 0.9$ because of a potential change in the late-stage reaction kinetics. The first-order kinetic model (Avrami–Erofe'ev, $n = 1$) gives the best fit to powder decomposition data over the widest range of values ($0.0 < \alpha < 0.8$). This model is different from the one we used in Johnson and Fegley (2000a, 2000b). The continued analysis of our previous and expanded data set led us to change our kinetic model for tremolite powder decomposition.

The larger tremolite grains most likely follow a different reaction model as indicated by the slightly different curves in the reduced time plots (see Fig. 4b). The best regression for the larger grain kinetic data occurs with the Avrami–Erofe'ev model, Eq. (3), where $n = 2$. If $n = 2$ and $n = \lambda + \beta$, we propose that λ (dimensional growth) is 2 and β (nucleation) is 0 (i.e., instantaneous nucleation). We used alpha values less than or equal to 0.7 at each temperature for these linear regressions.

After determining which kinetic models to follow, we calculated a rate constant for each set of experiments. The rate constant is given by the relationship $k = f(\alpha)/t$, where k is the rate constant (h^{-1}), t is time (h), and $f(\alpha)$ is the kinetic model. The calculated rate constants are listed in Table 3. Note that the rate constants for tremolite powder decomposition are different than those listed in Johnson and Fegley (2000a).

We used the Arrhenius relationship shown in Eq. (4) to calculate the temperature dependence of the rate constants. The Arrhenius equation is

$$k = A\mathrm{e}^{(-E_a/RT)}, \tag{4}$$

where A is the pre-exponential factor, T is the temperature in Kelvin, R is the gas constant, E_a is the activation energy ($kJ\,mol^{-1}$), and k is the rate constant (h^{-1}). The activation energy is generally considered to represent an energy barrier, and the pre-exponential factor has been interpreted as a reaction frequency (Galwey and Brown, 1999). The Arrhenius equation gives a linear relationship between the log of the rate constant and inverse temperature (Eq. (5)):

$$\log_{10} k\left(\mathrm{h}^{-1}\right) = \log_{10} A + \frac{-E_a}{R\ln 10} \cdot \frac{1}{T}. \tag{5}$$

This linearity allows us to extrapolate the rate to temperatures where it is difficult to measure rates in real time. Figure 5 shows an Arrhenius plot with our data and illustrates the gap between Venus' surface temperatures (e.g., 740 K in the lowlands) and those used in our experiments.

Table 3
Tremolite rate data used to calculate rate equations and activation energies

Temperature (K)	Rate constant, k (h^{-1}) $\times 10^{-3} \pm 1\sigma$
Powder exps, α: 0.0–0.8	
Equation (3), $n = 1$: nucleation and growth	
N_2 gas set[a]	
1237	171.3 ± 5.60
1213	62.51 ± 1.40
1202	60.36 ± 1.00
1177	23.92 ± 0.22
1150	4.651 ± 0.055
1122	2.506 ± 0.040
CO_2 gas set 1[a]	
1238	201.2 ± 3.8
1213	74.58 ± 1.08
1196	42.69 ± 0.73
1178	21.37 ± 0.25
1148	5.722 ± 0.11
1120	2.055 ± 0.040
1090	0.356 ± 0.021
CO_2 gas set 2[b]	
1224	227.0 ± 3.6
1212	166.8 ± 1.3
1176	45.90 ± 0.68
1152	19.62 ± 0.26
1103	1.462 ± 0.115
1073	0.395 ± 0.020
1023	0.024 ± 0.001
CO_2 gas set 3[c]	
1212	194.3 ± 1.9
1177	48.13 ± 0.35
1151	15.12 ± 0.79
1103	1.811 ± 0.013
1045	0.058 ± 0.001
Crystal exps, α: 0.0–0.7	
Equation (3), $n = 2$: nucleation and growth	
1224	59.98 ± 1.88
1212	49.68 ± 1.96
1176	10.18 ± 0.209
1148	3.306 ± 0.067
1104	0.340 ± 0.007

[a] Vertical furnace, cylindrical crucible.
[b] Horizontal furnace, combustion boat.
[c] Horizontal furnace, cylindrical crucible.

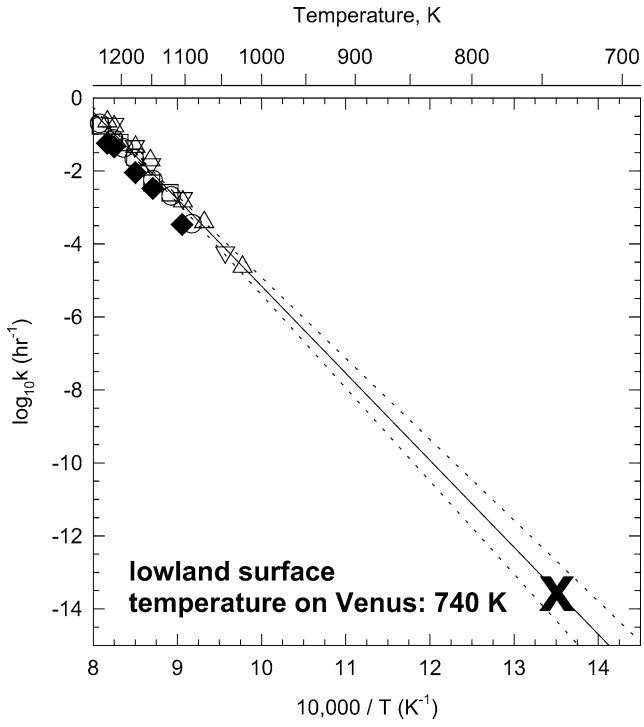

Fig. 5. Reaction rate constants versus $10{,}000/T$ shown in an Arrhenius plot. Key to symbols: [O] vertical furnace, CO_2 gas, cylindrical crucible; [□] vertical furnace, N_2 gas, cylindrical crucible; [▽] horizontal furnace, CO_2 gas, cylindrical crucible; [△] horizontal furnace, CO_2 gas, combustion boat. One sigma error is smaller than the size of the symbols. The solid diamonds are the rate constants for the tremolite crystal experiments. Table 3 lists the rate constants for both powder and crystal data and the rate equations are given in Eqs. (6) and (7). The solid line shows the linear regression of the tremolite powder decomposition and the dashed lines indicate the 95% confidence prediction interval of the regression.

Table 4 lists tremolite powder decomposition rate equations and activation energies associated with the different types of kinetic models. We present this information to illustrate the similar magnitudes of values among the equations. Nevertheless, we use the following equations to determine the decomposition rate of tremolite powder and tremolite crystals:

$$\log_{10} k_{\text{powder}}\left(\text{h}^{-1}\right) = 18.69(\pm 0.19) - 23{,}845(\pm 833)/T, \quad (6)$$

$$\log_{10} k_{\text{crystal}}\left(\text{h}^{-1}\right) = 19.82(\pm 0.07) - 25{,}670(\pm 916)/T. \quad (7)$$

The activation energies associated with these rate equations for tremolite powder and crystals are $456 \pm 16\ \text{kJ mol}^{-1}$ and $491 \pm 18\ \text{kJ mol}^{-1}$, respectively.

4. Tremolite decomposition mechanism

Previously proposed mechanisms for tremolite decomposition range from a simple description of the reaction (Thilo, 1939) to a statement of silica tetrahedra rearrangement with concurrent Ca and Mg interdiffusion (Xu et al., 1996). These are general descriptions of the reaction mechanism but do not specify reaction steps for the decomposition. Ideally, the mechanism should describe a series of physical steps needed for a particular reaction to proceed. We propose a series of steps for tremolite thermal decomposition using the following clues: atomic locations within the crystal lattice, physical changes, simultaneous or consecutive decomposition and dehydroxylation, activation energy of the reaction, bond lengths and strengths, and location of water formation. We begin by introducing tremolite's crystal structure.

Tremolite is composed of repeating double chains of silica tetrahedra (Si_4O_{11}) that run parallel to the c- or long axis (Whittaker, 1960). It is this double chain that gives tremolite its fibrous habit. Figure 6 shows structural schematics of tremolite from two different views. The top schematic is modified from a diagram given by Sueno et al. (1973) and highlights the tetrahedral double chain. The second schematic is a projection of the tremolite structure looking down the c-axis and is modified from a diagram given by Colville et al. (1966). The large A-sites, labeled within the schematics, are typically vacant in tremolite but can be 10- to 12-coordinated when occupied. These A-sites form channels that run parallel to the c-axis. The anion sites, O1 through O7, are typically filled with oxygen except for O3. The O3 sites contain hydroxyl groups (OH^-) and are located approximately in the center of the A-site vacancies at the level of the apical oxygen on the silica tetrahedra (O1 and O2). There are four cation sites: M1, M2, M3, and M4. The M4 site has 6- to 8-coordination, houses the larger Ca atom, and borders the A-site vacancy. The three remaining cation

Table 4
Tremolite *powder* decomposition rate equations and activation energies for different kinetic models ($\alpha = 0.0$–0.8)

Kinetic model	Model equation	Rate equation $\log_{10} k$ (h^{-1})	Activation energy E_a (kJ mol^{-1})
First-order reaction[a] (preferred model)	$-\ln(1-\alpha)$	18.69–23,845/T	456
Nucleation and growth ($n=2$)[b]	$(-\ln(1-\alpha))^{1/2}$	17.87–23,157/T	443
Nucleation and growth ($n=3$)[b]	$(-\ln(1-\alpha))^{1/3}$	17.52–22,912/T	439
Nucleation and growth ($n=4$)[b]	$(-\ln(1-\alpha))^{1/4}$	17.30–22,786/T	436
Contracting volume	$1-(1-\alpha)^{1/3}$	17.87–23,583/T	451
Diffusion[c]	$1-2\alpha/3-(1-\alpha)^{2/3}$	18.13–24,447/T	468

[a] Also Avrami–Erofe'ev model, $n=1$.
[b] Avrami–Erofe'ev model.
[c] Ginstling–Brounshtein model.

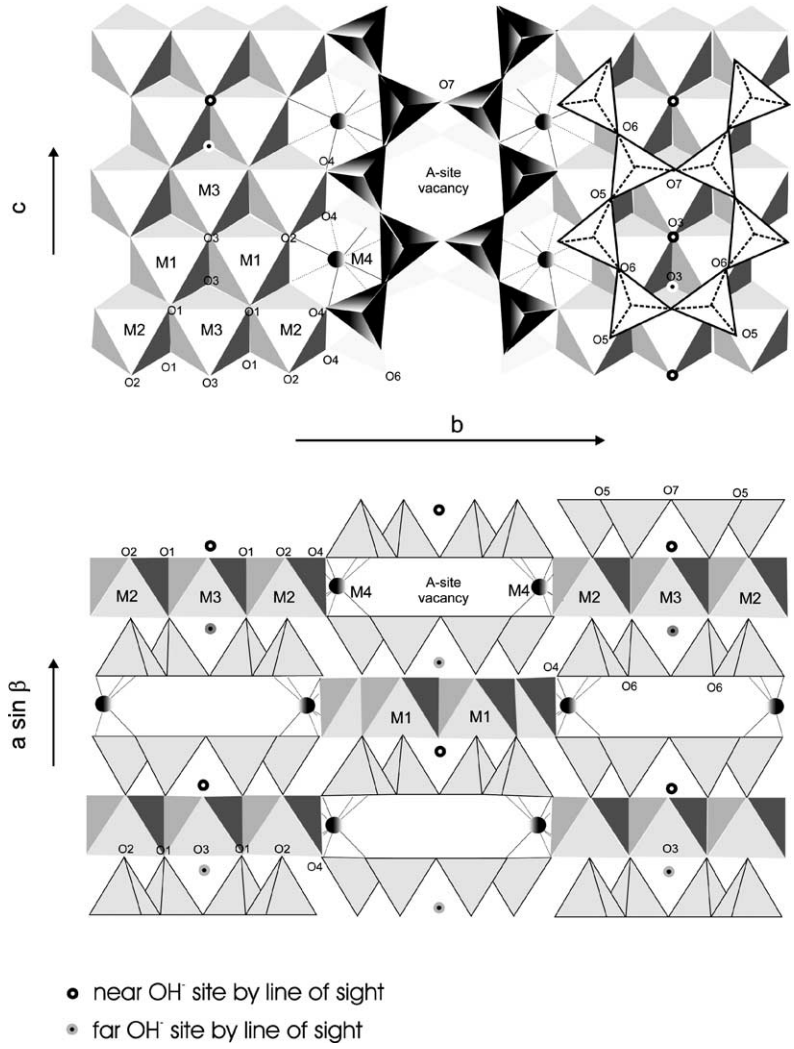

Fig. 6. Top and side views of the amphibole structure. The top schematic, modified from Sueno et al. (1973), looks down on the *c*-axis; the bottom diagram, modified from Colville et al. (1966), gives a side view of the structure along the *c*-axis. In each diagram, several sites are labeled. These sites and occupancies are described for ideal tremolite, $Ca_2Mg_5Si_8O_{22}(OH)_2$. The A-sites are typically vacant and form channels that run parallel to the *c*-axis. The anion sites, O1 through O7, are filled with oxygen except for O3. The O3 sites contain hydroxyls, OH pairs, and are located approximately in the center of the A-site vacancies at the level of the apical oxygen on the silica tetrahedra (O1 and O2). These hydroxyl sites are highlighted with solid circles with centered dots. There are four cation sites: M1, M2, M3, and M4. The M4 site contains Ca and the three remaining cation sites hold Mg. Hydroxyls are bound to M1 and M3 (both Mg sites). The tetrahedra are composed of single Si cations surrounded by four bridging oxygen atoms.

sites are Mg octahedra. OH pairs are bound to the M1 and M3 sites such that these Mg octahedra are each connected to four oxygen ions and two OH groups (O3 sites). Whittaker (1960), Colville et al. (1966), Sueno et al. (1973), and Klein and Hurlbut (1993) describe ion placement within the amphibole structure in greater detail.

A clue to the decomposition mechanism is tremolite's decomposition products: a mixture of two solid-solution pyroxenes, which are single-chain silicates, and a silica polymorph. If we view the tremolite structure shown in Fig. 6 simplistically, it appears straightforward to obtain a single chain pyroxene by unzipping the double chain along the *c*-axis. This splitting is an oversimplification but agrees with observations that the decomposition products retain tremolite's original *c*-axis orientation (Thilo, 1939; Freeman and Taylor, 1960; Freeman, 1962; Xu et al., 1996). The preferred two-dimensional growth of the decomposed regions along the *c*-axis (along the fiber) suggests structural control. We do not observe an intermediate step of anhydrous tremolite formation during decomposition. For example, during phlogopite decomposition at temperatures of $\sim 500^\circ$ C, a mica anhydride forms. This anhydride has essentially the same XRD pattern as the original phlogopite and can be rehydrated back to phlogopite. Complete decomposition or destruction of the mica structure requires temperatures greater than 1000° C (see discussion by Zolotov et al. (1997) and references therein). In the case of phlogopite mica, dehydroxylation and decomposition are consecutive rather than simultaneous. Conversely, we showed a 1:1 correlation between the decrease of the mid-IR hydroxyl peak and tremo-

lite mass loss in Johnson and Fegley (2000a, 2000b). We also found that pyroxene lines become stronger and tremolite lines weaker as water loss occurs. Studies by Freeman and Taylor (1960), Freeman (1962), and Patterson and O'Conner (1966) also report that tremolite decomposition occurs concurrently with dehydroxylation. The apparent simultaneous structural shift and loss of hydroxyl and absence of a tremolite anhydride suggest that decomposition and dehydroxylation are interdependent or are indistinguishable.

Both the activation energy and pre-exponential factor have the potential to constrain a reaction mechanism. A survey by Galwey (1994) shows that our pre-exponential values, while high, fall within the range of values reported for other solid-state thermal decomposition reactions. The pre-exponential factor (A in Eq. (4)) has been interpreted as a molecular collision frequency (in gas–gas reactions) or as a lattice vibration (Brown et al., 1980). Unfortunately, there is no consensus about the physical significance of the pre-exponential factor in solid decompositions (e.g., Galwey, 1994). Therefore, the pre-exponential factor is not discussed further. On the other hand, the activation energy, E_a, is generally acknowledged to represent a reaction barrier. These barriers can be physical (e.g., molecular diffusion through a layer), energetic (e.g., breaking and/or forming chemical bonds), or a combination of the two (Galwey and Brown, 1999). The magnitude of the E_a value may reflect the rate-limiting step, i.e., the process that takes the most energy to overcome. Gas diffusion through a reacted layer or a simple dehydration process usually results in a low activation energy, generally less than 150 kJ mol^{-1} for dehydration as seen for thermal decomposition of hydrated salts (see Brown et al. (1980, Table 10) and references therein).

Higher activation energies, such as seen here, indicate breaking of chemical bonds or ionic diffusion through a crystal lattice (Galwey and Brown, 1999). The ions in tremolite are Ca^{2+}, Mg^{2+}, Si^{4+}, O^{2-}, and OH^{-}. The E_a for interdiffusion of hydroxyl and fluorine in tremolite was measured as 41 kJ mol^{-1} under hydrothermal conditions (Brabander et al., 1995). The activation energy for hydrogen diffusion in amphiboles under hydrothermal conditions ranges from 67 to 105 kJ mol^{-1} (Graham et al., 1984). The measured value of E_a for oxygen self-diffusion under hydrothermal conditions in tremolite is 163 kJ mol^{-1} (Farver and Giletti, 1985) and 226 kJ mol^{-1} for diopside (Farver, 1989). Under anhydrous conditions, the E_a for oxygen self-diffusion in diopside was reported to be as high as 477 kJ mol^{-1} (McKeegan and Ryerson, 1990). The activation energy for silicon diffusion in enstatite was measured at 400 kJ mol^{-1} (Fisler et al., 1997). The E_a values for Mg self-diffusion under anhydrous conditions in enstatite range from 265 to 360 kJ mol^{-1} depending on the crystal axis (Schwandt et al., 1998). Diffusion of Ca and Mg in clinopyroxene under anhydrous conditions has an E_a of 360 kJ mol^{-1} (Brady and McCallister, 1983). In a review of measured pyroxene activation energies, Freer et al. (1982) calculated an E_a of 469 kJ mol^{-1} for Ca diffusion in pyroxenes under anhydrous conditions.

We measured an apparent activation energy of $\sim$ 460 kJ mol^{-1} for decomposition of tremolite powder. This value is about 35 kJ less than the activation energy measured for decomposition of tremolite crystals. We suspect that this difference reflects the extra energy needed to create nucleation sites on the crystals. The activation energies of both systems are relatively close to the other within error, so presumably the mechanism is the same for both. The E_a of $\sim$ 460 kJ mol^{-1} is comparable to the reported activation energies for Ca or oxygen diffusion in pyroxenes under anhydrous conditions. The reported activation energies for Si and Mg diffusion are $\sim$ 60 to 100 kJ mol^{-1} lower, respectively, than our E_a for tremolite decomposition.

We also note that the E_a of $\sim$ 460 kJ mol^{-1} is probably much higher than that needed for diffusion of molecular H_2O through the tremolite structure. The vacant A-sites that form channels within tremolite are individually large enough ($\sim$ 47–58 Å^3) to allow passage of a water molecule ($<$ 11–30 Å^3) and these sites expand during heating (Sueno et al., 1973). These channels are effective conduits for physical molecular diffusion, and if diffusion of H_2O were the rate-limiting step it would result in a low activation energy. Scanning electron microscopy of reacted tremolite indicates that water vapor diffusion should be rapid because the decomposed regions are very porous. If physical diffusion is not the rate-limiting step, then ionic diffusion is the probable reaction barrier.

The strength of the chemical bonds may also constrain the reaction mechanism. The bond strength and bond length are related so that when a chemical bond lengthens, the bond strength decreases (Cotton and Wilkinson, 1972). When tremolite is heated, the bonds between the cations and their respective oxygen atoms lengthen (refer to Sueno et al. (1973) for details). The largest bond stretching occurs in the M4 site that houses the 8-coordinated Ca^{2+} atom and has the longest bonds at room temperature. The 6-coordinated Mg^{2+} sites, M1, M2, and M3, are also stretched with M1 affected most and M3 least. Within the temperature range of our study, the changes in the Si–O bond length are insignificant; the silica tetrahedra appear to shift and the Si–O bonds do not break. Using this information, we can qualitatively state that Ca has the weakest bonds and silica has the strongest. We can also calculate the relative strengths of the different bonds by using the electrostatic valence rule as outlined by Pauling (1960). Pauling defined the electrostatic bond strength as the cation's valence charge divided by its coordination number and postulated that "in a stable ionic structure the valence of each anion…(equals)…the sum of the strengths of the electrostatic bonds to it from the adjacent cations." This rule also applies to silicate minerals. Of the three aforementioned bonds in tremolite (Si–O, Ca–O, and Mg–O), Ca–O has the weakest bond strength (using the forementional definition) with a value of 0.25. The bond strength values for Si–O and Mg–O in tremolite are 1.0 and 0.3, respectively. These values agree with our qualitative assessment that Ca has the weaker bonds. Phillips et al.

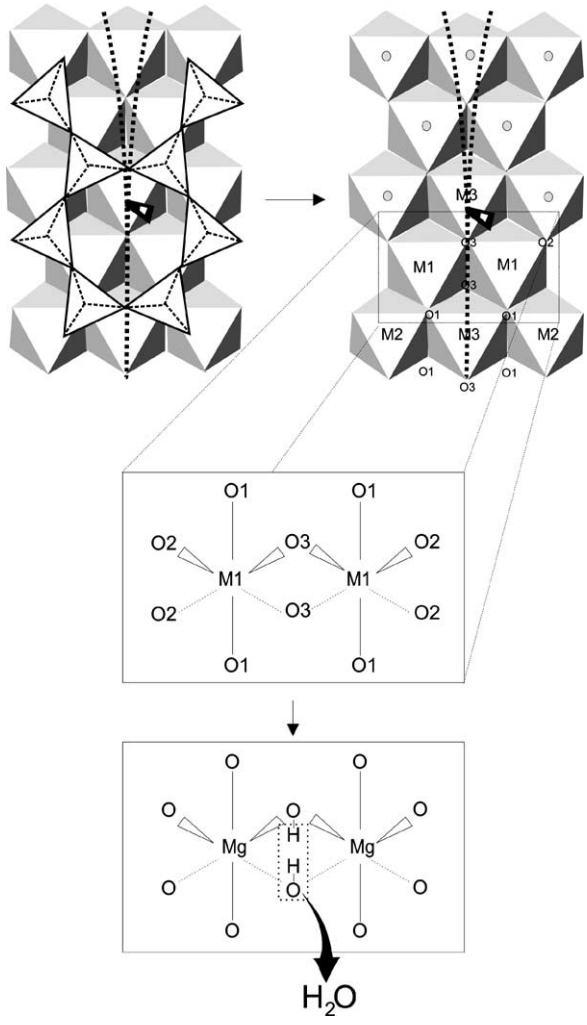

Fig. 7. A simplified view of the tremolite structure from Fig. 6 and a schematic of OH– and Mg– bonding. In this figure, the amphibole double chain is "unzipped" to form the pyroxene single chain. The M1 sites contain the closest neighboring hydroxyls in O3 sites that are located on opposite sides of the Mg– polyhedra layer and central to the A-site vacancies. During heating, we propose that these hydroxyls combine to form water, water escapes, and the remaining structure shifts to maintain electrical neutrality.

(1988) suggested that in riebeckites (double-chain silicates), the bond strength between OH and Mg (O3 site) is lowered. If the bond between OH and Mg is weakened, then the weakest bonds in tremolite are held by Ca–O and Mg–OH.

The mechanism of water formation during tremolite decomposition is also important. Wilkins and Vedder (1969) suggested that H^+ diffused to the surface to form water in Fe-bearing micas and amphiboles. This mechanism might be applicable for Fe oxidation but may not be viable for Fe-free tremolite because there is no oxidation. An alternative scenario for tremolite is that water forms in situ during decomposition and quickly escapes. To make a water molecule, we need two hydroxyls in close proximity. Hydroxyls exist in the O3 sites (see Fig. 6) and the two closest neighboring O3 sites are located on opposite sides of the same Mg–polyhedra layer. Figure 7 shows a simpler view of the tremolite structure and a schematic of the OH– and Mg– bonding. Each of the M1 sites contain two neighboring OH bonds as shown in the stick diagrams in Fig. 7. Of the three Mg polyhedra, the M1 site undergoes the greatest expansion; therefore, the M1 site should have the weaker bonds. At some point during heating, it is probable that it is more energetically favorable for the hydroxyls to combine and form water than to remain with the silicate structure. Once H_2O forms, the remaining bonds shift to maintain electrical neutrality. Once this adjustment begins, decomposition proceeds along the path of least resistance which appears to be along the A-site channels or *c*-axis. Calcium, the cation with the overall weakest bonds, borders the A-vacancies in the M4 site and is probably relatively quick to shift position. Alternatively, the Ca bond could break first, the structure shifts, and then water forms. It is unclear which bonds, Ca or Mg, break first but it is not surprising that decomposition and dehydroxylation are closely linked. The decomposition pattern suggests structural control and if indeed water forms as described, this provides an easy yet elegant method for unzipping the double-chain silica tetrahedra.

We rule out the breakdown of the Mg–OH bond as the rate-limiting step. Brucite, $Mg(OH)_2$, is a hydroxide where each Mg atom is octahedrally coordinated with OH. During decomposition, these bonds must be broken and the apparent activation energy of brucite decomposition is ~ 125 kJ mol^{-1} (Gordon and Kingery, 1967). This value is much lower than our measured E_a thus eliminating Mg–OH bond breaking as the main contributor to the activation energy for tremolite decomposition. Dehydroxylation and decomposition are simultaneous, which leads us to the scenario that water formation and release is rapid with the subsequent unzipping/rearrangement of the double chain serving as the rate-limiting step.

We propose the following thermal decomposition mechanism for tremolite:

(1) the atomic bonds undergo thermal expansion and the A-sites expand (Sueno et al., 1973),
(2) two adjacent hydroxyls on the Mg-M1 sites react to form water via $2OH^- \rightarrow H_2O + O^{2-}$,
(3) water escapes,
(4) the remaining cations undergo bond breaking/shifting/reforming with bridging oxygen, and
(5) silica tetrahedra shift to maintain electronic neutrality (single chains appear first then the more complex silica phase).

This mechanism would apply to both powder and crystal samples. We suspect that the activation energy of the powder decomposition is lower than that for the crystals because of the higher potential for nucleation caused by the powders' greater surface area and perhaps greater defect density introduced by grinding. It is unclear whether step 4 or 5 is rate limiting. The fifth step, tetrahedral shifting, cannot be eliminated as rate limiting but the fourth step is more probable

Table 5
Times for 50% decomposition using rate Eqs. (6) and (7) (see text)

Temperature (K)	Tremolite powder[a]	Tremolite crystals[a]
1200	(4 h) 11 h (27 h)	(18 h) 31 h (53 h)
1100	(11 days) 28 days (72 days)	(59 days) 113 days (216 days)
1000	(4 years) 11 years (33 years)	(22 years) 67 years (200 years)
900	(1300 years) 5000 years (19,000 years)	(8000 years) 48,000 years (290,000 years)
800	(2 Myr) 10 Myr (61 Myr)	(12 Myr) 175 Myr (3000 Myr)
740	(0.32 Gyr) 2.7 Gyr (23 Gyr)	(2.4 Gyr) 70 Gyr (2000 Gyr)

[a] Values within parentheses indicate the 95% confidence prediction interval of the calculated value.

because of the similarity of our E_a values with E_a values associated with ionic diffusion of Ca or oxygen.

5. Discussion

Tremolite longevity on Venus. Our expanded data set yields revised rate constants (Table 3) and new rate equations for tremolite thermal decomposition (Eqs. (6) and (7)). As shown by the Arrhenius plot in Fig. 5, there is a sizable gap between our experimental temperatures and Venus' surface temperatures. The rate equations are valid for the temperature range of the experiments and are explicitly assumed to be valid at the lower temperatures. We can extrapolate to these lower temperatures because cation diffusion in tremolite (as in all natural silicates) is probably in the extrinsic diffusion regime (Freer, 1981; Chakraborty et al., 1994). This means that defects due to impurities are greater than those inherent to absolutely pure tremolite. As a result, the apparent activation energy (the slope) is constant because there is no transition from the intrinsic diffusion regime (thermally generated defects in absolutely pure tremolite) to the extrinsic diffusion regime. Table 5 lists the times required for 50% decomposition of powder and crystal tremolite at different temperatures. There are two key points to take away from this table:

(1) decomposition slows dramatically as the temperature decreases, and
(2) the larger tremolite crystals take longer to decompose by an order of magnitude compared to the tremolite powder.

The second point supports our statement in Johnson and Fegley (2000a) that decomposition is slower for larger grain sizes. This finding has direct implications for tremolite survival in rocks. Tremolite found in terrestrial metamorphic rocks is typically larger than powder (e.g., millimeter- versus micrometer-sized particulates); therefore, we expect tremolite grains in rocks to have lifetimes like those of our crystals instead of our powders. The 50% decomposition time for tremolite powder (micrometer-sized grains) at Venus' surface temperature of 740 K is 2.7 Gyr. This value is shorter than the previous result of 4 Gyr presented in Johnson and Fegley (2000a). On an absolute scale, 2.7 Gyr is still a very long time, bearing in mind that complete decomposition takes up to 10 times longer (see normalized time plots in Fig. 5). In an ongoing experiment, a tremolite powder sample heated for approximately 4 years at 740 K has not decomposed. This sample is still "cooking" but we do not expect any changes. These results strengthen our previous conclusions from Johnson and Fegley (2000a, 2000b) that tremolite can survive on Venus over geologic time scales at current surface conditions.

Tremolite decomposition at Venus' surface pressure. The atmospheric pressure on Venus' surface is 95.6 bar (at the modal planetary radius) (Ford and Pettengill, 1992) or about 100 times greater than the surface pressure on Earth. According to our proposed mechanism, the tremolite decomposition rate is determined by a combination of bond breaking and ionic movement which is limited by energy barriers that are breached at higher temperatures. The molar volume of tremolite decreases by 0.01% at Venus's surface pressure. (Tremolite's bulk modulus is 850 kbar (Comodi et al., 1991).) Comodi et al. (1991) suggest that the pressure-induced volume change is a result of polyhedral tilting and show that tremolite is more easily compressed along the a-axis. In other words, higher pressure reduces the size of the A-site vacancies whereas temperature has the opposite effect (Sueno et al., 1973). The $\sim 0.01\%$ volume decrease should have an insignificant effect on ionic diffusion and structural rearrangement in tremolite. In support of this suggestion, there is very little change in the Mg^{2+} diffusion coefficient in forsterite at 100-bar pressure (see Chakraborty et al., 1994, Fig. 4). We predict that the tremolite decomposition rate and its apparent activation energy are unaffected by Venus' surface pressure under anhydrous conditions.

Acknowledgments

We thank the reviewers for their constructive comments. We also thank K. Lodders for helpful suggestions, A. Hofmeister for generous use of the IR spectrometer, and D. Kremser, R. Poli, and P. Swan for technical assistance. This work was supported by Grant NAG5-4565 from the NASA Planetary Atmospheres Program.

Appendix A

Table A.1
Tremolite dehydroxylation experiments in CO_2, with vertical furnaces and cylindrical crucibles

Experiment	Time (h)	Mass loss (mg)	Fraction reacted[a] (α)
Temperature: 1238 K, initial mass: 103.678 mg			
e45a	1.0	0.874	0.347
e45b	2.0	1.187	0.472
e45c	3.0	1.427	0.567
e45d	4.5	1.726	0.686
e45e	6.0	1.911	0.760
e45f	8.0	2.083	0.828
e45g	11.0	2.234	0.888
e45h	16.0	2.348	0.933
e45i	24.0	2.411	0.959
e45j	37.0	2.449	0.974
Temp: 1213 K, initial mass: 98.037 mg			
e44a	1.0	0.557	0.234
e44b	2.5	0.781	0.328
e44c	4.0	0.943	0.396
e44d	6.0	1.152	0.484
e44e	9.25	1.431	0.602
e44f	13.5	1.685	0.708
e44g	19.0	1.901	0.799
e44h	26.0	2.049	0.862
e44i	36.0	2.160	0.908
e44j	49.0	2.222	0.934
e44k	67.0	2.246	0.944
e44l	92.0	2.284	0.960
Temperature: 1196 K, initial mass: 102.507 mg			
e42a	1.0	0.508	0.204
e42b	2.5	0.664	0.267
e42c	4.5	0.833	0.335
e42d	9.25	1.146	0.461
e42e	17.25	1.524	0.613
e42f	25.25	1.790	0.720
e42g	35.75	2.016	0.811
e42h	44.0	2.120	0.852
e42i	53.0	2.194	0.882
e42j	66.0	2.266	0.911
e42k	82.0	2.310	0.929
e42l	103.0	2.326	0.935
e42m	135.0	2.367	0.952
e42n	180.0	2.379	0.957
Temperature: 1178 K, initial mass: 89.238 mg			
e39a	1.0	0.417	0.193
e39b	2.62	0.505	0.233
e39c	4.15	0.574	0.265
e39d	6.15	0.645	0.298
e39e	10.15	0.793	0.366
e39f	16.23	0.940	0.434
e39g	25.23	1.145	0.529
e39h	40.23	1.436	0.663
e39i	62.23	1.699	0.785
e39j	85.23	1.851	0.855
e39k	109.25	1.947	0.899
e39l	134.25	1.996	0.922
e39m	163.25	2.021	0.934
e39n	186.42	2.032	0.939
Temperature: 1148 K, initial mass: 132.642 mg			
e41a	1.0	0.442	0.137
e41b	3.0	0.518	0.161
e41c	5.0	0.565	0.176
e41d	11.5	0.679	0.211
e41e	28.5	0.931	0.289
e41f	52.5	1.227	0.381
e41g	89.0	1.573	0.489
e41h	127.7	1.891	0.588
e41i	411.9	2.827	0.879
e41j	617.98	2.937	0.913
e41k	783.48	3.001	0.933
e41l	942.48	3.017	0.938
e41m	1036.58	3.027	0.941
Temperature: 1120 K, initial mass: 98.192 mg			
e40a	1.0	0.307	0.129
e40b	3.0	0.358	0.150
e40c	7.0	0.389	0.163
e40d	16.2	0.445	0.187
e40e	31.2	0.506	0.212
e40f	53.2	0.591	0.248
e40g	97.8	0.742	0.311
e40h	141.8	0.887	0.372
e40i	189.63	1.041	0.437
e40j	248.38	1.187	0.498
e40k	532.46	1.753	0.736
e40l	738.46	1.916	0.804
e40m	770.46	1.940	0.814
e40n	962.46	2.060	0.865
e40o	1198.46	2.127	0.893
e40p	1366.46	2.169	0.911
e40q	1696.46	2.217	0.931
Temperature: 1090 K, initial mass: 97.328 mg			
e43a	1.0	0.238	0.101
e43b	5.75	0.300	0.127
e43c	17.25	0.338	0.143
e43d	42.0	0.383	0.162
e43e	104.0	0.438	0.186
e43f	174.0	0.470	0.199
e43g	297.0	0.552	0.234
e43h	513.0	0.687	0.291
e43i	645.0	0.777	0.329
e43j	1071.0	0.937	0.397

[a] Calculated using max % mass loss: 2.426 wt% (3 pts, $1\sigma = 0.041$).

Table A.2
Tremolite dehydroxylation experiments in N_2, with vertical furnaces and cylindrical crucibles

Experiment	Time (h)	Mass loss (mg)	Fraction reacted[a] (α)
Temperature: 1237 K, initial mass: 97.659 mg			
e52a	1.0	0.796	0.336
e52b	2.0	1.042	0.440
e52c	3.0	1.289	0.544
e52d	5.0	1.613	0.681
e52e	7.5	1.847	0.780
e52f	11.0	2.049	0.865
e52g	16.0	2.166	0.914
e52h	24.0	2.266	0.956
Temperature: 1213 K, initial mass: 93.443 mg			
e50a	1.0	0.505	0.223
e50b	2.5	0.698	0.308
e50c	4.75	0.907	0.400
e50d	8.25	1.195	0.527
e50e	14.0	1.526	0.673
e50f	22.0	1.792	0.790
e50g	30.0	1.926	0.850
e50h	38.0	2.024	0.893
e50i	54.0	2.098	0.925
Temperature: 1202 K, initial mass: 94.231 mg			
e49a	1.0	0.494	0.216
e49b	2.5	0.686	0.300
e49c	4.75	0.896	0.392
e49d	8.25	1.169	0.511
e49e	14.0	1.500	0.656
e49f	22.0	1.784	0.780
e49g	30.0	1.925	0.842
e49h	38.0	2.022	0.884
e49i	54.0	2.104	0.920
Temperature: 1177 K, initial mass: 103.845 mg			
e53a	1.0	0.431	0.171
e53b	3.25	0.574	0.228
e53c	7.50	0.784	0.311
e53d	14.0	1.018	0.404
e53e	22.0	1.285	0.510
e53f	37.0	1.656	0.657
e53g	55.0	1.951	0.774
e53h	80.0	2.147	0.852
e53i	129.0	2.300	0.913
Temperature: 1150 K, initial mass: 93.361 mg			
e54a	1.0	0.318	0.140
e54b	4.5	0.384	0.170
e54c	10.0	0.453	0.200
e54d	21.0	0.540	0.238
e54e	41.0	0.702	0.310
e54f	71.0	0.916	0.404
e54g	111.0	1.150	0.508
e54h	160.25	1.379	0.609
e54i	212.25	1.551	0.685
e54j	286.0	1.753	0.774
e54k	382.0	1.902	0.840
e54l	502.0	2.014	0.889
e54m	648.0	2.074	0.916
e54n	816.0	2.111	0.932
e54o	1050.0	2.135	0.943
Temperature: 1122 K, initial mass: 95.955 mg			
e55a	1.0	0.307	0.132
e55b	4.5	0.375	0.161
e55c	10.0	0.422	0.181
e55d	21.0	0.482	0.207
e55e	41.0	0.589	0.253
e55f	71.0	0.724	0.311
e55g	119.0	0.917	0.394
e55h	181.0	1.121	0.482
e55i	253.0	1.302	0.559
e55j	349.0	1.514	0.650
e55k	482.0	1.735	0.745
e55l	648.0	1.895	0.814
e55m	846.0	2.023	0.869
e55n	1113.0	2.099	0.902

[a] Calculated using max % mass loss: 2.426 wt% (3 pts, $1\sigma = 0.041$).

Table A.3
Tremolite dehydroxylation experiments in CO_2, with horizontal furnaces and combustion boats

Experiment	Time (h)	Mass loss (mg)	Fraction reacted[a] (α)	Experiment	Time (h)	Mass loss (mg)	Fraction reacted[a] (α)
Temperature: 1224 K, initial mass: 90.940 mg				Temperature: 1152 K, initial mass: 96.756 mg			
e58a	1.0	0.779	0.353	e67a	1.0	0.406	0.173
e58b	2.0	1.078	0.489	e67b	5.0	0.586	0.250
e58c	3.0	1.319	0.598	e67c	15.0	0.927	0.395
e58d	4.05	1.479	0.670	e67d	30.0	1.289	0.549
e58e	5.0	1.632	0.740	e67e	47.0	1.572	0.670
e58f	6.0	1.753	0.795	e67f	74.0	1.890	0.805
e58g	8.0	1.931	0.875	e67g	113.0	2.057	0.876
e58h	11.0	2.076	0.941	e67h	161.0	2.136	0.910
e58i	15.0	2.099	0.951	e67i	207.0	2.163	0.921
e58j	21.0	2.167	0.982	e67j	278.0	2.220	0.946
e58k	45.0	2.178	0.987	e67k	377.0	2.223	0.947
Temperature: 1212 K, initial mass: 119.299 mg				Temperature: 1103 K, initial mass: 108.891 mg			
e71a	1.0	0.873	0.302	e60a	144.0	0.957	0.362
e71b	2.5	1.327	0.459	e60b	505.0	1.725	0.653
e71c	4.75	1.825	0.631	e60c	935.0	2.114	0.800
e71d	8.0	2.265	0.783	e60d	1410.0	2.258	0.855
e71e	13.75	2.578	0.891	e60e	1884.0	2.403	0.910
e71f	20.0	2.693	0.930				
e71g	27.0	2.764	0.955	Temperature: 1073 K, initial mass: 102.732 mg			
e71h	43.0	2.792	0.965	e61a	144.0	0.509	0.204
e71i	68.0	2.801	0.968	e61b	504.0	0.757	0.304
				e61c	934.0	0.992	0.398
Temperature: 1176 K, initial mass: 92.528 mg				e61d	1408.0	1.167	0.468
e63a	1.0	0.460	0.205	e61e	1910.0	1.438	0.577
e63b	3.0	0.641	0.286	e61f	2503.0	1.624	0.652
e63c	7.0	0.904	0.403	e61g	3585.0	2.001	0.803
e63d	17.0	1.378	0.614	e61h	4757.0	2.205	0.885
e63e	25.0	1.661	0.740	e61i	6531.0	2.301	0.923
e63f	41.0	1.919	0.855	e61j	9219.0	2.359	0.947
e63g	61.0	2.055	0.915				
e63h	82.0	2.069	0.922	Temperature: 1023 K, initial mass: 99.495 mg			
e63i	179.0	2.134	0.951	e97a	1508.0	0.405	0.168
				e97b	3215.0	0.474	0.196
				e97c	4823.0	0.530	0.220
				e97d	7031.0	0.645	0.267
				e97e	9687.0	0.750	0.311
				e97f	12689.0	0.866	0.359

[a] Calculated using max % mass loss: 2.426 wt% (3 pts, $1\sigma = 0.041$).

Table A.4
Tremolite dehydroxylation experiments in CO_2, with horizontal furnaces and cylindrical crucibles

Experiment	Time (h)	Mass loss (mg)	Fraction reacted[a] (α)
Temperature: 1212 K, initial mass: 97.796 mg			
e70a	1.0	0.771	0.325
e70b	2.5	1.168	0.492
e70c	4.75	1.599	0.674
e70d	8.0	1.944	0.819
e70e	13.75	2.179	0.918
e70f	20.0	2.269	0.956
e70g	27.0	2.320	0.978
e70h	43.0	2.332	0.983
e70i	68.0	2.335	0.984
Temperature: 1177 K, initial mass: 91.546 mg			
e62a	1.0	0.456	0.205
e62b	3.0	0.636	0.286
e62c	7.0	0.911	0.410
e62d	17.0	1.402	0.631
e62e	25.0	1.670	0.752
e62f	41.0	1.938	0.873
e62g	61.0	2.052	0.924
e62h	84.0	2.107	0.949
e62i	179.0	2.131	0.960
Temperature: 1151 K, initial mass: 102.698 mg			
e66a	1.0	0.436	0.175
e66b	5.0	0.631	0.253
e66c	15.0	0.953	0.383
e66d	30.0	1.276	0.512
e66e	47.0	1.565	0.628
e66f	74.0	1.810	0.726
e66g	113.0	2.143	0.860
e66h	161.0	2.250	0.903
e66i	207.0	2.302	0.924
e66j	278.0	2.383	0.956
e66k	378.0	2.398	0.962
Temperature: 1103 K, initial mass: 98.256 mg			
e64a	25.0	0.449	0.188
e64b	47.0	0.518	0.217
e64c	96.0	0.691	0.290
e64d	162.0	0.875	0.367
e64e	260.0	1.112	0.467
e64f	400.0	1.413	0.593
e64g	593.0	1.689	0.709
e64h	857.0	1.948	0.817
e64i	1240.0	2.125	0.891
e64j	1739.0	2.207	0.926
e64k	2771.0	2.246	0.942
Temperature: 1045 K, initial mass: 96.055 mg			
e73a	286.0	0.385	0.165
e73b	618.0	0.446	0.191
e73c	1149.0	0.507	0.218
e73d	1889.0	0.595	0.255
e73e	2966.0	0.677	0.291
e73f	5080.0	0.827	0.355
e73g	7412.0	1.011	0.434
e73h	10783.0	1.228	0.527
e73i	14480.0	1.440	0.618
e73j	18346.0	1.671	0.717
e73k	22545.0	1.817	0.780
e73l	27030.0	1.943	0.834

[a] Calculated using max % mass loss: 2.426 wt% (3 pts, $1\sigma = 0.041$).

Table A.5
Tremolite crystal dehydroxylation experiments in CO_2, with horizontal furnaces and combustion boats

Experiment	Time (h)	Mass loss (mg)	Fraction reacted[a] (α)	Experiment	Time (h)	Mass loss (mg)	Fraction reacted[a] (α)
Temperature: 1224 K, initial mass: 35.673 mg				Temperature: 1148 K, initial mass: 93.891 mg			
e57a	1.0	0.106	0.122	e68a	1.0	0.079	0.035
e57b	2.25	0.157	0.182	e68b	15.0	0.123	0.054
e57c	4.0	0.224	0.259	e68c	46.0	0.265	0.116
e57d	7.0	0.373	0.431	e68d	85.0	0.491	0.216
e57e	11.0	0.520	0.600	e68e	139.0	0.794	0.349
e57f	15.0	0.641	0.741	e68f	213.0	1.244	0.546
e57g	19.0	0.749	0.866	e68g	326.0	1.640	0.720
e57h	24.0	0.836	0.966	e68h	494.0	1.901	0.835
e57i	31.0	0.867	1.001	e68i	756.0	2.035	0.893
e57j	37.0	0.867	1.001	e68j	1116.0	2.068	0.908
e57k	58.0	0.867	1.001	e68k	1666.0	2.068	0.908
Temperature: 1212 K, initial mass: 108.884 mg				Temperature: 1104 K, initial mass: 113.336 mg			
e72a	1.0	0.387	0.147	e65a	23.0	0.146	0.053
e72b	2.5	0.548	0.207	e65b	45.0	0.169	0.061
e72c	4.75	0.825	0.312	e65c	96.0	0.192	0.070
e72d	8.0	1.212	0.459	e65d	186.0	0.241	0.088
e72e	13.75	1.728	0.654	e65e	309.0	0.326	0.119
e72f	20.0	2.092	0.792	e65f	545.0	0.484	0.176
e72g	27.0	2.332	0.883	e65g	902.0	0.758	0.276
e72h	43.0	2.493	0.944	e65h	1498.0	1.222	0.444
e72i	68.0	2.584	0.978	e65i	2220.0	1.691	0.615
e72j	118.0	2.609	0.988	e65j	3372.0	2.143	0.779
e72k	207.0	2.628	0.995	e65k	4543.0	2.287	0.832
				e65l	7640.0	2.486	0.904
Temperature: 1176 K, initial mass: 99.358 mg							
e69a	2.0	0.188	0.078				
e69b	13.0	0.378	0.157				
e69c	32.5	0.742	0.308				
e69d	56.5	1.229	0.510				
e69e	97.0	1.758	0.729				
e69f	145.0	2.019	0.838				
e69g	194.0	2.149	0.892				
e69h	261.0	2.225	0.923				
e69i	359.0	2.263	0.939				
e69j	474.0	2.274	0.943				

[a] Calculated using max % mass loss: 2.426 wt% (3 pts, $1\sigma = 0.041$).

References

Boyd, F.R., Schairer, J.F., 1964. The system $MgSiO_3$–$CaMgSi_2O_6$. J. Petrol. 5, 275–309.

Brabander, D.J., Hervig, R.L., Jenkins, D.M., 1995. Experimental determination of F–OH interdiffusion in tremolite and significance to flourine-zoned amphiboles. Geochim. Cosmochim. Acta 59 (17), 3549–3560.

Brady, J.B., McCallister, R.H., 1983. Diffusion data for clinopyroxenes from homogenization and self-diffusion experiments. Am. Mineral. 68, 95–105.

Brown, M.E., Dollimore, D., Galwey, A.K., 1980. Reactions in the solid state. In: Bamford, C.H., Tipper, C.F.H. (Eds.), Comprehensive Chemical Kinetics, Vol. 22. Elsevier, Amsterdam.

Carlson, W.D., 1986. Reversed pyroxene phase equilibria in a CaO–MgO–SiO_2 from 925° to 1,175° C at one atmosphere pressure. Contrib. Mineral. Petrol. 92, 218–224.

Chakraborty, S., Farver, J.R., Yund, R.A., Rubie, D.C., 1994. Mg tracer diffusion in synthetic forsterite and San Carlos olivine as a function of P, T and fO_2. Phys. Chem. Minerals 21, 489–500.

Clark, M.W., 1966. The Kinetics and Mechanism of the Dehydroxylation of Crocidolite. MSc thesis. Victoria University of Wellington, Wellington, New Zealand.

Clark, M.W., Freeman, A.G., 1967. Kinetics and mechanism of dehydroxylation of crocidolite. Trans. Faraday Soc. 63, 2051–2056.

Colville, P.A., Ernst, W.G., Gilbert, M.C., 1966. Relationships between cell parameters and chemical compositions of monoclinic amphiboles. Am. Mineral. 51, 1727–1754.

Comodi, P., Mellini, M., Ungaretti, L., Zanazzi, P.F., 1991. Compressibility and high pressure structure refinement of tremolite, pargasite, and glaucophane. Eur. J. Mineral. 3, 485–499.

Cotton, F.A., Wilkinson, G., 1972. Advanced Inorganic Chemistry: A Comprehensive Text. Wiley, New York.

Deer, W.A., Howie, R.A., Zussman, J., 1997. Rock-Forming Minerals, Vol. 2B. Geological Society, London.

Donahue, T.M., Grinspoon, D.H., Hartle, R.E., Hodges, R.R., 1997. Ion/neutral escape of hydrogen and deuterium: evolution of water. In: Bougher, S.W., Hunten, D.M., Phillips, R.J. (Eds.), Venus II. Univ. of Arizona Press, Tucson, pp. 385–414.

Farver, J.R., 1989. Oxygen self-diffusion in diopside with application to cooling rate determinations. Earth Planet. Sci. Lett. 92, 386–396.

Farver, J.R., Giletti, B.J., 1985. Oxygen diffusion in amphiboles. Geochim. Cosmochim. Acta 49, 1403–1411.

Fisler, D.K., Mackwell, S.J., Petschl, S., 1997. Grain boundary diffusion in enstatite. Phys. Chem. Minerals 24, 264–273.

Ford, P.G., Pettengill, G.H., 1992. Venus topography and kilometer-scale slopes. J. Geophys. Res. 97, 13103–13114.

Freeman, A.G., Taylor, H.W.F., 1960. Die Entwässerung von Tremolit. Silikattechn. 11 (8), 390–392.

Freeman, A.G., 1962. Chemical and crystallographic studies of amphiboles. PhD thesis. University of Aberdeen, Aberdeen, United Kingdom.

Freeman, A.G., 1966. The dehydroxylation behavior of amphiboles. Mineral. Mag. 35, 953–957.

Freer, R., 1981. Diffusion in silicate minerals and glasses: a data digest and guide to the literature. Contrib. Mineral. Petrol. 76, 440–454.

Freer, R., Carpenter, M.A., Long, J.V.P., Reed, S.J.B., 1982. "Null result" diffusion experiments with diopside: implications for pyroxene equilibria. Earth Planet. Sci. Lett. 58, 285–292.

Galwey, A.K., 1994. Magnitudes of Arrhenius parameters for decomposition reactions of solids. Thermochim. Acta 242, 259–264.

Galwey, A.K., Brown, M.E., 1999. Thermal Decomposition of Ionic Solids. Elsevier, Amsterdam.

Ghose, S., 1981. Subsolidus reactions and microstructures in amphiboles. In: Veblen, D.R. (Ed.), Amphiboles and Other Hydrous Pyriboles—Mineralogy. Mineralogical Society of America, Washington, DC, pp. 325–372.

Gordon, R.S., Kingery, W.D., 1967. Thermal decomposition of brucite: II, Kinetics of decomposition in vacuum. J. Am. Ceram. Soc. 50 (1), 8–14.

Graham, C.M., Harmon, R.S., Sheppard, S.M.F., 1984. Experimental hydrogen isotope studies: hydrogen isotope exchange between amphibole and water. Am. Mineral. 69, 128–138.

Hodgson, A.A., 1965. The thermal decomposition of amosite. Mineral. Mag. 35, 445–463.

Hodgson, A.A., Freeman, A.G., Taylor, H.F.W., 1965. The thermal decomposition of crocidolite from Koegas, South Africa. Mineral. Mag. 35, 5–30.

Johnson, N.M., 2002. Tremolite Decomposition and Water on Venus. PhD thesis. Washington University in Saint Louis, Saint Louis, MO.

Johnson, N.M., Fegley Jr., B., 2000a. Water on Venus: new insights from tremolite decomposition. Icarus 146, 301–306.

Johnson, N.M., Fegley Jr., B., 2000b. Tremolite decomposition and water on Venus. Lunar. Planet. Sci. 31. Abstract 1083.

Johnson, N.M., Fegley Jr., B., 2003. Longevity of fluorine-bearing tremolite on Venus. Icarus, in press.

Klein, C., Hurlbut Jr., C.S., 1993. Manual of Mineralogy. Wiley, New York.

McKeegan, K.D., Ryerson, F.J., 1990. Diffusion of oxygen in diopside and spinel: implications for oxygen isotopic anomalies in CAIs. Lunar. Planet. Sci. 21, 775–776. Abstract.

Patterson, J.H., O'Conner, D.J., 1966. Chemical studies of amphibole asbestos. Aust. J. Chem. 19, 1155–1164.

Pauling, L., 1960. The Nature of the Chemical Bond and the Structure of Molecules and Crystals: An Introduction to Modern Structural Chemistry. Cornell Univ. Press, Ithaca, NY.

Phillips, M.W., Popp, R.K., Clowe, C.A., 1988. Structural adjustments accompanying oxidation-dehydrogenation in amphiboles. Am. Mineral. 73, 500–506.

Posnjak, E., Bowen, N.L., 1931. The role of water in tremolite. Am. J. Sci. 222, 203–214.

Schwandt, C.S., Cygan, R.T., Westrich, H.R., 1998. Magnesium self-diffusion in orthoenstatite. Contrib. Mineral. Petrol. 130, 390–396.

Sosman, R.B., 1965. The Phases of Silica. Rutgers Univ. Press., New Brunswich, NJ.

Sueno, S., Cameron, M., Papike, J.J., Prewitt, C.T., 1973. The high temperature crystal chemistry of tremolite. Am. Mineral. 58, 649–664.

Thilo, E., 1939. Chemische Untersuchungen von Silikaten. IX. Die Umwandlung von Tremolit in Diopsid beim Erhitzen. Z. Kristallographie 101, 345–350.

Vermaas, F.H.S., 1952. The amphibole asbestos of South Africa. Trans. Geol. South Africa 55, 199–232.

Whittaker, E.J.W., 1960. The crystal chemistry of the amphiboles. Acta Crystallogr. 13, 291–298.

Wilkins, R.W.T., Vedder, W., 1969. Mechanisms of thermal decomposition in the micas and amphiboles. In: Mitchell, J.W., DeVries, R.C., Roberts, R.W., Cannon, P. (Eds.), Reactivity of Solids. Wiley–Interscience, New York, pp. 227–236.

Wittels, M., 1951. Structural transformations in amphiboles at elevated temperatures. Am. Mineral. 36, 851–858.

Wittels, M., 1952. The structural disintegration of some amphiboles. Am. Mineral. 52, 28–36.

Xu, H., Veblen, D.R., Luo, G., Xue, J., 1996. Transmission electron microscopy of the thermal decomposition of tremolite into clinopyroxene. Am. Mineral. 81, 1126–1132.

Zolotov, M.Yu., Fegley Jr., B., Lodders, K., 1997. Hydrous silicates and water on Venus. Icarus 130, 475–494.